



# LUND UNIVERSITY

## A comprehensive model for ultrawideband propagation channels

Molisch, Andreas; Balakrishnan, Kannan; Cassioli, Dajana; Chong, Chia-Chin; Emami, Shahriar; Fort, Andrew; Kåredal, Johan; Kunisch, Juergen; Schantz, Hans; Siwiak, Kazimierz

*Published in:*

[Host publication title missing]

*DOI:*

[10.1109/GLOCOM.2005.1578452](https://doi.org/10.1109/GLOCOM.2005.1578452)

2005

[Link to publication](#)

*Citation for published version (APA):*

Molisch, A., Balakrishnan, K., Cassioli, D., Chong, C.-C., Emami, S., Fort, A., Kåredal, J., Kunisch, J., Schantz, H., & Siwiak, K. (2005). A comprehensive model for ultrawideband propagation channels. In *[Host publication title missing]* (Vol. 6, pp. 3648-3653). IEEE - Institute of Electrical and Electronics Engineers Inc.. <https://doi.org/10.1109/GLOCOM.2005.1578452>

*Total number of authors:*

10

### General rights

Unless other specific re-use rights are stated the following general rights apply:

Copyright and moral rights for the publications made accessible in the public portal are retained by the authors and/or other copyright owners and it is a condition of accessing publications that users recognise and abide by the legal requirements associated with these rights.

- Users may download and print one copy of any publication from the public portal for the purpose of private study or research.
- You may not further distribute the material or use it for any profit-making activity or commercial gain
- You may freely distribute the URL identifying the publication in the public portal

Read more about Creative commons licenses: <https://creativecommons.org/licenses/>

### Take down policy

If you believe that this document breaches copyright please contact us providing details, and we will remove access to the work immediately and investigate your claim.

LUND UNIVERSITY

PO Box 117  
221 00 Lund  
+46 46-222 00 00

# A Comprehensive Model for Ultrawideband Propagation Channels

Andreas F. Molisch, *Fellow, IEEE*, Kannan Balakrishnan, *Member, IEEE* Dajana Cassioli, *Member, IEEE*  
Chia-Chin Chong, *Member, IEEE* Shahriar Emami, *Senior Member, IEEE*  
Andrew Fort, *Member, IEEE* Johan Karedal, *Student Member, IEEE* Juergen Kunisch, *Member, IEEE*  
Hans Schantz, *Member, IEEE*, and Kazimierz Siwiak, *Senior Member, IEEE*

**Abstract**— This paper describes a comprehensive statistical model for UWB propagation channels that is valid for a frequency range from 3–10 GHz. It is based on measurements and simulations in the following environments: residential indoor, office indoor, built-up outdoor, industrial indoor, farm environments, and body area networks. The model is independent of the used antennas. It includes the frequency dependence of the pathloss, as well as several generalizations of the Saleh-Valenzuela model, like mixed Poisson times of arrival and delay dependent cluster decay constants. The model can thus be used for realistic performance assessment of UWB systems. It was accepted by the IEEE 802.15.4a working group (WG) as standard model for evaluation of UWB system proposals.

## I. INTRODUCTION

Ultrawideband (UWB) communications systems have many attractive properties, including low interference to and from other wireless systems, low sensitivity to fading, easier wall-and floor penetration, and inherent security [1], [2], [3]. UWB communications originally started with the spark-gap transmitter of Hertz and Marconi. However, it was not until the 1990s that the interest was renewed. The pioneering work in [4], [5], [6], [7] developed the concept of time-hopping impulse radio (TH-IR) systems. In 2002, the frequency regulator in the USA allowed unlicensed UWB transmission (subject to the fulfillment of a spectral masks), and other countries are expected to follow suit. One of the most promising applications for UWB are sensor networks, where the good ranging and geolocation capabilities of UWB [8] are particularly useful. The data rates for those applications are typically low (<1 Mbit/s). Recognizing these developments the IEEE has established the standardization group 802.15.4a, which is currently in the process of developing a standard for these applications.

The ultimate performance limits of any communications system are determined by the channel it operates in. For a UWB system, this is the UWB propagation channel, which differs from conventional (narrowband) propagation in many respects. The performance of a system thus can only be evaluated when realistic channel models are available. A number of UWB channel models have been proposed in the past: [9] suggested a model for the frequency range below 1 GHz (this model was adopted by the 802.15.4a group for testing of low-frequency UWB systems). The IEEE 802.15.3a group developed a channel model [10] that is valid from 3 – 10 GHz, but is designed only for indoor residential and office environments, and the distance between transmitter and receiver is restricted to < 10 m.

A considerable number of papers has been published on the measurement and modeling for specific environments (see [11] for an overview), but none of them has gained widespread acceptance for system testing purposes.

In the present paper, we present a general model for UWB channels that is valid for the high-frequency range (3 – 10 GHz) in a number of different environments, based on measurements and simulations of the authors [12], [13], [14], [15] and other papers in the open literature. The model has been developed by the authors during their work for the 802.15.4a group, and was accepted by that body as the official model for comparing different system proposals for standardization. The value of the present paper is thus twofold:

- It represents a model for UWB channels that is accepted by an official standardization body for the purpose of selecting among physical layer proposals, and is available for large number of environments.
- It includes a number of refinements and improvements beyond what the authors and others had previously presented in the literature, specifically
  - frequency dependence of the pathloss, and thus implicitly the distortions of each separate multipath component (MPCs);
  - modeling of the number of clusters of multipath components in the Saleh-Valenzuela model as a random variable;
  - a power delay profile that models a "soft" onset, so that the first arriving paths can be considerably weaker than later MPCs; this is critical for accurate assessment of ranging capabilities of UWB;
  - a new model for body area networks that includes correlated lognormal shadowing.

The remainder of the paper is organized as follows: in Sec. II, we present the generic channel model structure, especially discussing the refinements compared to previous literature. Section III describes the actual parameterization in different environments, while Sec. IV concentrates on the channel model for body area networks, which has a slightly different underlying structure. Section V shows some example results for power delay profiles and other parameters characterizing the delay dispersion. A summary concludes the paper.

## II. GENERIC CHANNEL MODEL

### A. Environments

The following environments have the most importance for sensor network applications, and are the ones for which the model is parameterized

- 1) *Indoor residential*: these environments are critical for "home networking", linking different appliances, as well as safety (fire, smoke) sensors over a relatively small area. The building structures of residential environments are characterized by small units, with indoor walls of reasonable thickness.
- 2) *Indoor office*: some of the rooms are comparable in size to residential, but other rooms (especially cubicle areas, laboratories, etc.) are considerably larger. Areas with many small offices are typically linked by long corridors. Each of the offices typically contains furniture, bookshelves on the walls, etc., which adds to the attenuation given by the (often thin) office partitionings.
- 3) *Outdoor*: while a large number of different outdoor scenarios exist, the current model covers only a suburban-like microcell scenario, with a rather small range.
- 4) *Industrial environments*: are characterized by larger enclosures (factory halls), filled with a large number of metallic reflectors. This is anticipated to lead to severe multipath.
- 5) *Agricultural areas/farms*: for those areas, few propagation obstacles (silos, animal pens), with large distances in between, are present. The delay spread can thus be anticipated to be smaller than in other environments
- 6) *Body-area network (BAN)*: communication between devices located on the body, e.g., for medical sensor communications, "wearable" cellphones, etc.

The measurements and simulations that form the basis of the model in the different environments cover different frequency ranges. For the use within the IEEE standardization, they are defined to be used for the whole 2 – 10 GHz range. However, from a scientific point of view, they should only be used in the frequency range for which the underlying measurements are valid; those frequency ranges are specified in Sec. III. A similar statement is true for the distance between transmitter (TX) and receiver (RX) over which the model should be used.

### B. Pathgain

We define the *frequency-dependent path gain* (related to wideband path gain [16], [17]) in a UWB channel as

$$G(f, d) = E \left\{ \int_{f-\Delta f/2}^{f+\Delta f/2} |H(\tilde{f}, d)|^2 d\tilde{f} \right\} \quad (1)$$

where  $H(f, d)$  is the transfer function from antenna connector to antenna connector,  $\Delta f$  is chosen small enough so that diffraction coefficients, dielectric constants, etc., can be considered constant within that bandwidth,  $d$  is the distance between transmitter and receiver, and the expectation  $E\{\}$  is taken over the small-scale and large-scale fading.

To simplify computations, we assume that the path gain as a function of the distance and frequency can be written as a product of the terms

$$G(f, d) = G(f)G(d). \quad (2)$$

The frequency dependence of the channel path gain is modeled as [18], [19]

$$\sqrt{G(f)} \propto f^{-\kappa} \quad (3)$$

The distance dependence of the path gain in dB is described by the conventional power law

$$G(d) = G_0 - 10n \log_{10} \left( \frac{d}{d_0} \right) \quad (4)$$

where the reference distance  $d_0$  is set to 1 m,  $L_0$  is the path gain at the reference distance. The path gain exponent  $n$  depends on whether a line-of-sight (LOS) connection exists between the transmitter and receiver or not.

The path gain also depends on the antenna gains and efficiencies. Since these also contain a frequency dependence, the following equation is used for computing the total received power (this includes several simplifications and assumptions not reproduced here for space reasons - for details see [20]):

$$G(f) = \frac{1}{2} G_0 \eta_{\text{TX-ant}}(f) \eta_{\text{RX-ant}}(f) \frac{(f/f_c)^{-2(\kappa+1)}}{(d/d_0)^n}. \quad (5)$$

The total path gain shows random variations (due to shadowing), which are lognormally distributed, so that Eq. (4) is replaced by

$$G(d) = G_0 - 10n \log_{10} \left( \frac{d}{d_0} \right) + S \quad (6)$$

where  $S$  is a Gaussian-distributed random variable with zero mean and standard deviation  $\sigma_S$ .<sup>1</sup>

### C. Power delay profile (PDP)

The impulse response (in complex baseband) of the SV (Saleh-Valenzuela) model is given in general as [21]

$$h_{discr}(t) = \sum_{l=0}^L \sum_{k=0}^K a_{k,l} \exp(j\phi_{k,l}) \delta(t - T_l - \tau_{k,l}), \quad (7)$$

where  $a_{k,l}$  is the tap weight of the  $k^{th}$  component in the  $l^{th}$  cluster,  $T_l$  is the delay of the  $l^{th}$  cluster,  $\tau_{k,l}$  is the delay of the  $k^{th}$  MPC relative to the  $l^{th}$  cluster arrival time  $T_l$ . The phases  $\phi_{k,l}$  are uniformly distributed, i.e., for a bandpass system, the phase is taken as a uniformly distributed random variable from the range  $[0, 2\pi]$ . Deviating from the standard SV model, the number of clusters  $L$  is modeled as Poisson-distributed with probability density function (pdf)

$$pdf_L(L) = \frac{(\bar{L})^L \exp(-\bar{L})}{L!} \quad (8)$$

<sup>1</sup>For the simulations within the 802.15.4a standardization, the shadowing is not to be taken into account.

so that the mean  $\bar{L}$  completely characterizes the distribution. This modification gave better agreement with some of the experimental results used in this study.

By definition, we have  $\tau_{0,l} = 0$ . The distributions of the cluster arrival times are given by a Poisson processes

$$p(T_l|T_{l-1}) = \Lambda_l \exp[-\Lambda_l(T_l - T_{l-1})], \quad l > 0 \quad (9)$$

where  $\Lambda_l$  is the cluster arrival rate (assumed to be independent of  $l$ ). The classical SV model also uses a Poisson process for the ray arrival times. Due to the discrepancy in the fitting for the indoor residential, indoor office, and outdoor environments, we propose to model ray arrival times with mixtures of two Poisson processes as follows

$$p(\tau_{k,l}|\tau_{(k-1),l}) = \beta\lambda_1 \exp[-\lambda_1(\tau_{k,l} - \tau_{(k-1),l})] + (\beta - 1)\lambda_2 \exp[-\lambda_2(\tau_{k,l} - \tau_{(k-1),l})], \quad k > 0 \quad (10)$$

where  $\beta$  is the mixture probability, while  $\lambda_1$  and  $\lambda_2$  are the ray arrival rates.

For some environments, most notably the industrial environment, a "dense" arrival of multipath components was observed, i.e., each resolvable delay bin contains significant energy. In that case, the concept of ray arrival rates loses its meaning, and a realization of the impulse response based on a tapped delay line model with regular tap spacings is to be used.

The next step is the determination of the cluster powers and cluster shapes. The PDP (mean power of the different paths) is exponential within each cluster

$$E\{|a_{k,l}|^2\} \propto \Omega_l \exp(-\tau_{k,l}/\gamma_l) \quad (11)$$

where  $\Omega_l$  is the integrated energy of the  $l$ th cluster, and  $\gamma_l$  is the intra-cluster decay time constant.

The cluster decay rates are found to depend linearly on the arrival time of the cluster,

$$\gamma_l \propto k_\gamma T_l + \gamma_0 \quad (12)$$

where  $k_\gamma$  describes the increase of the decay constant with delay.

The mean (over the cluster shadowing) mean (over the small-scale fading) energy (normalized to  $\gamma_l$ ), of the  $l$ -th cluster follows in general an exponential decay

$$10 \log(\Omega_l) = 10 \log(\exp(-T_l/\Gamma)) + M_{cluster} \quad (13)$$

where  $M_{cluster}$  is a normally distributed variable with standard deviation  $\sigma_{cluster}$ .

For the NLOS case of some environments (office and industrial), the shape of the power delay profile can be different, namely (on a log-linear scale)

$$E\{|a_{k,1}|^2\} \propto (1 - \chi \cdot \exp(-\tau_{k,1}/\gamma_{rise})) \cdot \exp(-\tau_{k,1}/\gamma_1) \quad (14)$$

Here, the parameter  $\chi$  describes the attenuation of the first component, the parameter  $\gamma_{rise}$  determines how fast the PDP increases to its local maximum, and  $\gamma_1$  determines the decay at later times.

Residential	LOS	NLOS
valid range of $d$	7 – 20 m	7 – 20 m
Path gain		
$G_0$ [dB]	-43.9	-48.7
$n$	1.79	4.58
$S$ [dB]	2.22	3.51
$\kappa$	1.12 ± 0.12	1.53 ± 0.32
Power delay profile		
$\bar{L}$	3	3.5
$\Lambda$ [1/ns]	0.047	0.12
$\lambda_1, \lambda_2$ [1/ns], $\beta$	1.54, 0.15, 0.095	1.77, 0.15, 0.045
$\Gamma$ [ns]	22.61	26.27
$k_\gamma$	0	0
$\gamma_0$ [ns]	12.53	17.50
$\sigma_{cluster}$ [dB]	2.75	2.93
Small-scale fading		
$m_0$ [dB]	0.67	0.69
$\hat{m}_0$ [dB]	0.28	0.32
$\tilde{m}_0$	NA	NA
Office	LOS	NLOS
valid range of $d$	3 – 28 m	3 – 28 m
Path gain		
$n$	1.63	3.07
$\sigma_S$	1.9	3.9
$G_0$ [dB]	-35.4	-59.9
$\kappa$	0.03	0.71
Power delay profile		
$\bar{L}$	5.4	1
$\Lambda$ [1/ns]	0.016	NA
$\lambda_1, \lambda_2$ [1/ns], $\beta$	0.19, 2.97, 0.0184	NA
$\Gamma$ [ns]	14.6	NA
$k_\gamma$	0	NA
$\gamma_0$ [ns]	6.4	NA
$\sigma_{cluster}$ [dB]	3	NA
Small-scale fading		
$m_0$	0.42 dB	0.50 dB
$\hat{m}_0$	0.31	0.25
$\tilde{m}_0$	NA	NA
$\chi$	NA	0.86
$\gamma_{rise}$	NA	15.21
$\gamma_1$	NA	11.84

#### D. Small-scale fading

The distribution of the small-scale amplitudes is Nakagami

$$pdf(x) = \frac{2}{\Gamma(m)} \left(\frac{m}{\Omega}\right)^m x^{2m-1} \exp\left(-\frac{m}{\Omega}x^2\right), \quad (15)$$

where  $m \geq 1/2$  is the Nakagami  $m$ -factor,  $\Gamma(m)$  is the gamma function, and  $\Omega$  is the mean-square value of the amplitude. A conversion to a Rice distribution is approximately possible [22]. The  $m$ -parameter is modeled as a lognormally distributed random variable, whose logarithm has a mean  $m_0$  and standard deviation  $\hat{m}_0$ . For the first component of each cluster, the Nakagami factor is modeled differently. It is assumed to be deterministic and independent of delay

$$m = \tilde{m}_0 \quad (16)$$

A uniformly distributed phase is ascribed to all MPCs. Note that this passband representation is different from both [10] and [9], which used a (real) baseband model.

### III. MODEL PARAMETERIZATION

The parameters of the model are extracted by fitting measurement data to the model described in Sec. II. <sup>2</sup> The model for residential environments was extracted based on measurements that cover a range from 7 – 20 m, up to 10 GHz [13]. For office environments, the model was based on measurements that cover a range from 3 – 28 m, 2 – 8 GHz [14]. For outdoor, the measurements cover a range from 5 – 17 m, 3 – 6 GHz [15]. The derivation of the model and a description of the simulations (for the farm area) can be found in [23]. The model for industrial environments was extracted based on measurements [12] that cover a frequency range from 3 – 10 GHz and a distance range from 2 – 8 m, though the pathloss also relies on values from the literature [26].

From a scientific point of view, the parameterization is valid only for the range over which measurement data are available. Note, however, that for the comparison purposes within the IEEE 802.15.4a standardization group, the parameterization is used for the whole 2 – 10 GHz range, and also for all distances of interest.

Outdoor	LOS	NLOS	Farm
valid range of $d$	5 – 17 m	5 – 17 m	
Path gain			
$n$	1.76	2.5	1.58
$\sigma_S$	0.83	2	3.96
$G_0$	-45.6	-73.0	-48.96
$\kappa$	0.12	0.13	0
Power delay profile			
$\bar{L}$	13.6	10.5	3.31
$\Lambda$ [1/ns]	0.0048	0.0243	0.0305
$\lambda_1$ [1/ns]	0.27	0.15	0.0225, 0, 0
$\lambda_2$ [1/ns]	2.41	1.13	
$\beta$	0.0078	0.062	
$\Gamma$ [ns]	31.7	104.7	56
$k_\gamma$	0	0	0
$\gamma_0$ [ns]	3.7	9.3	0.92
$\sigma_{\text{cluster}}$ [dB]			3
Small-scale fading			
$m_0$	0.77 dB	0.56 dB	4.1 dB
$\hat{m}_0$	0.78	0.25	2.5 dB
$\tilde{m}_0$	NA	NA	0

<sup>2</sup>For extensive discussions about physical interpretations, see [1], [13], [14], [15], [23], [11], [25].

Industrial	LOS	NLOS
valid range of $d$	2 – 8 m	2 – 8 m
Path gain		
$n$	1.2	2.15
$\sigma_S$ [dB]	6	6
$G_0$ [dB]	-56.7	-56.7
$\kappa$	-1.103	-1.427
Power delay profile		
$\bar{L}$	4.75	1
$\Lambda$ [1/ns]	0.0709	NA
$\lambda$ [1/ns]	NA	NA
$\Gamma$	13.47	NA
$k_\gamma$	0.926	NA
$\gamma_0$	0.651	NA
$\sigma_{\text{cluster}}$ [dB]	4.32	NA
Small-scale fading		
$m_0$	0.36 dB	0.30 dB
$\hat{m}_0$	1.13	1.15
$\tilde{m}_0$ dB	12.99	
$\chi$	NA	1
$\gamma_{\text{rise}}$ [ns]	NA	17.35
$\gamma_1$ [ns]	NA	85.36

### IV. BODY AREA NETWORK

Section II presented a generic channel model representing typical indoor and outdoor environments for evaluating 802.15.4a systems. However, simulations and measurements of the radio channel around the human body indicate that some modifications are necessary to accurately model a body area network (BAN) scenario. Due to the extreme close range and the fact that the antennas are worn on the body, the BAN channel model has different path loss, amplitude distribution, clustering, and inter-arrival time characteristics compared with the other application scenarios within the 802.15.4a context.

Analysis of the electromagnetic field near the body using a finite difference time domain (FDTD) simulator indicated that in the 2 – 6 GHz range, no energy is penetrating through the body. Rather, pulses transmitted from an antenna diffract around the body and can reflect off of arms and shoulders. Thus, distances between the transmitter and receiver in our path loss model are defined as the distance *around* the perimeter of the body, rather than the straight-line distance *through* the body. The amplitude distributions measured near the body are also different: the log-normal distribution turned out to be best. In addition, the uncorrelated scattering assumption is violated for systems where both the transmitter and receiver are placed on the same body. Our simulations and measurements in an anechoic chamber indicate that there are always two clusters of multi path components due to the initial wave diffracting around the body, and a reflection off of the ground (more clusters could occur in an indoor environment due to reflections from walls etc., but this is not included in the model). Thus, the number of clusters is always 2 and does not need to be defined as a stochastic process as in the other scenarios. Furthermore, the inter-cluster arrival times are also deterministic and depend on the exact position of the transmitters on the body. To simplify this, we have assumed a fixed average inter-cluster arrival time depending on

the specified scenario. The very short transmission distances result in inter-path arrival times that are shorter than the delay resolution of the considered systems; thus a "dense" model (uniformly spaced tapped delay line) was used. The extracted channel parameters depended on the position of the receiver on the body. To incorporate this effect easily without having to perform a large number of simulations, only three scenarios are defined, corresponding to a receiver placed on the 'front', 'side', and 'back' of the body. The distance ranges for those environments are 0.04 – 0.17 m, 0.17 – 0.38 m, and 0.38 – 0.64 m, respectively.

Implementing this model on a computer involves generating  $N$  correlated lognormal variables representing the  $N$  different bins, and then applying an appropriate path loss based on the distance between the antennas around the body. This can be accomplished by generating  $N$  correlated normal variables, adding the pathloss, and then converting from a dB to linear scale as follows:

$$Y_{dB} = \mathbf{X} \cdot \text{chol}(\mathbf{C}) - \mathbf{M} - G_{dB} \quad (17)$$

$\mathbf{X}$  is a vector of  $N$  uncorrelated, unit-mean, unit-variance, normal variables. To introduce the appropriate variances and cross-correlation coefficients, this vector is multiplied by the upper triangular cholesky factorization of the desired covariance matrix  $\mathbf{C}$ . The means (a vector  $\mathbf{M}$ ) of each different bin and the large scale path loss ( $P_{dB}$ ) are subtracted.

The path gain can be calculated according to the following formula:

$$G_{dB} = -\gamma(d - d_0) + G_{0,dB} \quad (18)$$

with  $\gamma$  in units of dB/meter. The parameters of this path loss model extracted from the simulator and measurements are summarized in Table I. The means and variances of the lognormal distribution describing the amplitude distributions of each bin are given in Table II; the covariance matrices  $\mathbf{C}$  are not reproduced here for space reasons; they can be found in [20]. The arrival time between the first and second cluster is 8.7 ns for the 'front' scenario, 8.0 ns for the 'side' scenario, and 7.4 ns for the 'back' scenario. The inter-ray arrival time is fixed to 0.5 ns, as the simulation bandwidth for this channel model is only 2 GHz.

Parameter for BAN	Value
$\gamma$	107.8 dB/m
$d_0$	0.1 m
$G_0$	-35.5 dB

TABLE I  
PATHLOSS MODEL FOR BAN.

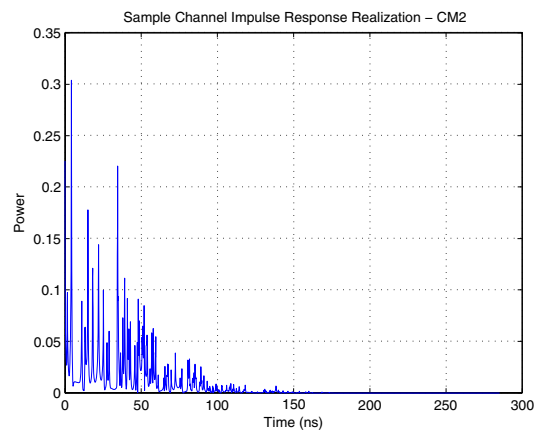


Fig. 1. Impulse response realization in CM2 (residential NLOS).

mean and variance of lognormal distribution for BAN						
Bin	front $\mu_{dB}/2$	front $\sigma_{dB}/2$	side $\mu_{dB}/2$	side $\sigma_{dB}/2$	back $\mu_{dB}/2$	back $\sigma_{dB}/2$
1	5.7	4.7	9.6	6.3	9.2	6.3
2	12.1	4.2	12.9	5.7	12.0	6.5
3	17.0	5.2	16.8	5.2	14.6	6.3
4	20.7	5.1	19.6	5.0	15.1	5.7
5	23.2	5.1	19.6	5.0	18.2	5.4
6	25.6	4.5	24.1	4.8	20.9	5.7
7	28.4	4.6	26.7	5.0	22.7	5.5
8	31.4	4.6	28.9	5.0	23.9	5.2
9	34.5	4.8	30.9	5.2	24.0	5.1
10	37.1	4.7	32.4	5.6	24.9	5.4

## V. SIMULATION RESULTS

The parameterized channel models can be used to generate ensembles of impulse responses, which in turn are employed to test the performance of different UWB transceiver structures. In the following, we present some example realizations, as well as parameters that allow insight into the effects of the impulse response on Rake receivers, which are used for combining different MPCs in both impulse-radio based systems and direct-sequence spread spectrum systems.

The impulse responses in different environments have some noticeable differences between them. Figure 1 depicts a typical impulse response in a residential NLOS situation (CM2). We see clearly the separation between the MPCs, and the arrival in clusters. This arises from the use of the SV model (with modified MPC arrival statistics) as described in Sec. II. A strong contrast to this is the impulse responses in the industrial NLOS environment in Fig. 2. In this example, we first observe that the first arriving MPC is strongly attenuated, and the maximum in the instantaneous power delay profile  $|h(\tau)|^2$  occurs only after about 50 ns. This is especially significant for ranging geolocation applications, since the ranging requires the detection of the *first* path, not of the strongest path. Detection of such a weak component in a noisy environment can be quite challenging.

A key parameter for Rake receivers is the number of "significant" MPCs. By this, we mean the number of MPCs that are

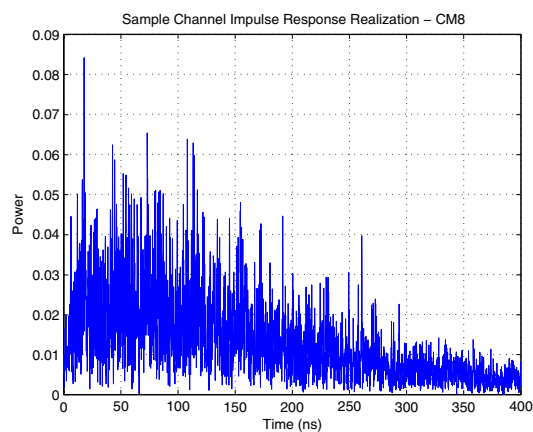


Fig. 2. Impulse response realization in CM8 (industrial NLOS).

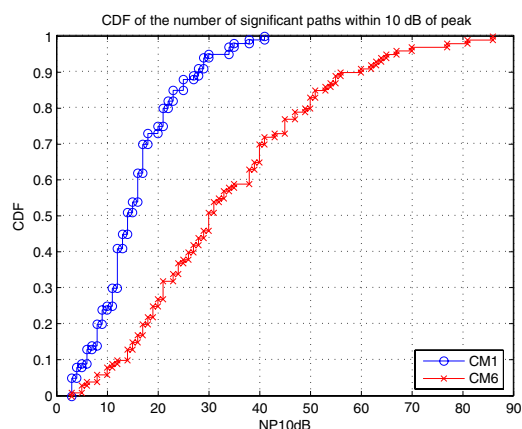


Fig. 3. Cumulative distribution function of the number of paths within 10dB of the strongest path in CM1 (residential LOS) and CM6 (outdoor NLOS).

within a certain dynamic range (e.g., 10 dB) of the strongest MPC in an impulse response. Figure 3 shows the cumulative distribution function of the number of significant paths for the residential LOS (CM1) and outdoor NLOS (CM6) environments.

The above figures are only a small sample of the results that can be obtained with this channel model. Extensive simulations of some 20 different systems have been performed as part of the IEEE 802.15.4a standardization activities.

## VI. SUMMARY AND CONCLUSIONS

We have presented a comprehensive model for UWB propagation channels that was accepted as standardized model by IEEE 802.15.4a. The model is based on a large number of measurement and simulation campaigns, and includes the most important propagation effects in UWB channels, including the frequency selectivity of the pathloss, stochastic interarrival times of the MPCs, and a soft onset of the power delay profile in some NLOS situations. The model allows to test a wide variety of UWB transceivers in a unified and reproducible way.

**Acknowledgment:** Stimulating discussions with the IEEE 802.15.4a working group, and the support by its chairman Pat

Kinney and vice chair Jason Ellis are gratefully acknowledged. The critical reading of the manuscript by Ulrich Schuster is gratefully acknowledged.

## REFERENCES

- [1] M. G. diBenedetto, T. Kaiser, A. F. Molisch, I. Oppermann, C. Politano, and D. Porcino (editors), *UWB communications systems Ū a comprehensive overview*. EURASIP publishing, 2005.
- [2] R. C. Qiu, H. Liu, and X. Shen, "Ultra-wideband for multiple access communications," *IEEE Communications Magazine*, vol. 43, pp. 80–87, 2005.
- [3] L. Yang and G. B. Giannakis, "Ultra-wideband communications - an idea whose time has come," *IEEE Signal Processing Magazine*, vol. 21, pp. 26–54, 2004.
- [4] L. Fullerton, "Time domain transmission system," U. S. Patent 4813057, 1989.
- [5] R. A. Scholtz, "Multiple access with time-hopping impulse modulation," in *Proc. IEEE MILCOM*, pp. 447–450, 1993.
- [6] M. Z. Win and R. A. Scholtz, "Impulse radio: How it works," *IEEE Comm. Lett.*, vol. 2, pp. 36–38, Feb 1998.
- [7] M. Z. Win and R. A. Scholtz, "Ultra-wide bandwidth time-hopping spread-spectrum impulse radio for wireless multiple-access communications," *IEEE Trans. Comm.*, vol. 48, pp. 679–691, Apr 2000.
- [8] S. Geczi, Z. Tian, G. B. Giannakis, Z. Sahinoglu, H. Kobayashi, A. F. Molisch, and H. V. Poor, "Localization via ultra-wideband radios," *IEEE Communications Magazine*, vol. 43, pp. 70–84, July 2005.
- [9] D. Cassioli, M. Z. Win, and A. F. Molisch, "The ultra-wide bandwidth indoor channel: from statistical model to simulations," *IEEE J. Selected Areas Comm.*, vol. 20, pp. 1247–1257, 2002.
- [10] A. F. Molisch, J. R. Foerster, and M. Pendergrass, "Channel models for ultrawideband personal area networks," *IEEE Personal Communications Magazine*, vol. 10, pp. 14–21, Dec. 2003.
- [11] A. F. Molisch, "Ultrawideband propagation channels - theory, measurement, and models," (invited paper) *IEEE Trans. Vehicular Techn.*, special issue on UWB, in press, 2005.
- [12] J. Karedal, S. Wyne, P. Almers, F. Tufvesson, and A. F. Molisch, "Statistical analysis of the UWB channel in an industrial environment," in *Proc. VTC fall 2004*, pp. 81–85, 2004.
- [13] C. C. Chong, Y. Kim, and S. S. Lee, "A modified S-V clustering channel model for the UWB indoor residential environment," in *Proc. IEEE VTC spring 05*, 2005.
- [14] B. Kannan et al., "UWB channel characterization in office environments," Tech. Rep. Document IEEE 802.15-04-0439-00-004a, 2004.
- [15] B. Kannan et al., "UWB channel characterization in outdoor environments," Tech. Rep. Document IEEE 802.15-04-0440-00-004a, 2004.
- [16] G. Kadel and R. Lorenz, "Impact of the radio channel on the performance of digital mobile communication systems," in *Proc. IEEE Int. Symp. on Personal, Indoor and Mobile Radio Communications (PIMRC)'95*, pp. 419–423, 1995.
- [17] J.-P. Rossi, "Influence of measurement conditions on the evaluation of some radio channel parameters," *IEEE Trans. on Vehicular Technology*, vol. 48, pp. 1304–1316, 1999.
- [18] R. Qiu and I.-T. Lu, "Wideband wireless multipath channel modeling with path frequency dependence," in *IEEE International Conference on Communications (ICC'96)*, 1996.
- [19] R. C. Qiu and I. Lu, "Multipath resolving with frequency dependence for broadband wireless channel modeling," *IEEE Trans. Veh. Tech.*, 1999.
- [20] A. F. Molisch et al., "IEEE 802.15.4a channel model – final report," Tech. Rep. Document IEEE 802.15-04-0662-02-004a, 2005.
- [21] A. Saleh and R. A. Valenzuela, "A statistical model for indoor multipath propagation," *IEEE J. Selected Areas Comm.*, vol. 5, pp. 138–137, Feb. 1987.
- [22] G. L. Stueber, *Principles of Mobile Communication*. Kluwer, 1996.
- [23] S. Emami et al. Tech. Rep. Document, 2005.
- [24] A. F. Molisch, "UWB propagation channels," in *UWB communications systems Ū a comprehensive overview* (T. Kaiser, ed.), p. in press, Eurasip, 2004.
- [25] K. Siwiak, H. Bertoni, and S. M. Yano, "Relation between multipath and wave propagation attenuation," *Electronics Letters*, vol. 39, pp. 142–143, 2003.
- [26] T. S. Rappaport, S. Y. Seidel, and K. Takamizawa, "Statistical channel impulse response models for factory and open plan building radio communication system design," *IEEE Trans. Comm.*, vol. 39, pp. 794–807, 1991.